Mechanism of Rapid Electron Transfer during Oxygen Activation in the R2 Subunit of *Escherichia coli* Ribonucleotide Reductase. 2. Evidence for and Consequences of Blocked Electron Transfer in the W48F Variant

Carsten Krebs,[§] Shuxian Chen,[§,‡] Jeffrey Baldwin,[†] Brenda A. Ley,[†] Utpal Patel,[†] Dale E. Edmondson,[⊥] Boi Hanh Huynh,[§] and J. Martin Bollinger, Jr.*[,†]

Contribution from the Department of Biochemistry and Molecular Biology, The Pennsylvania State University, University Park, Pennsylvania 16802, and the Departments of Physics, Biochemistry and Chemistry, Emory University, Atlanta, Georgia 30322

Received April 12, 2000

Abstract: The mechanism and outcome of dioxygen activation by the carboxylate-bridged diiron(II) cluster in the W48F site-directed variant of protein R2 of ribonucleotide reductase from *Escherichia coli* has been investigated by kinetic, spectroscopic, and chemical methods. The data corroborate the hypothesis advanced in earlier work and in the preceding paper that W48 mediates, by a shuttling mechanism in which it undergoes transient one-electron oxidation, the transfer of the "extra" electron that is required for formation of the formally Fe(IV)Fe(III) cluster **X** on the reaction pathway to the tyrosyl radical/μ-oxodiiron(III) cofactor of the catalytically active protein. The transient 560-nm absorption, which develops in the reaction of the wild-type R2 protein and is ascribed to the W48 cation radical, is not observed in the reaction of R2-W48F. Instead, a diradical intermediate containing both **X** and the Y122 radical (**X**-Y$^\bullet$) accumulates rapidly to a high level. The formation of this **X**-Y$^\bullet$ species is demonstrated indirectly by optical, Mössbauer, and EPR kinetic data, which show concomitant accumulation of the two constituents, and directly by the unique EPR and Mössbauer spectroscopic features of the **X**-Y$^\bullet$ species, which can be properly simulated by using the known magnetic properties of **X** and Y122$^\bullet$ and introducing a spin−spin interaction between the two radicals. This analysis of the spectroscopic data provides an estimate of the distance between the two radical constituents that is consistent with the crystallographically defined distance between Y122 and the diiron cluster. These results suggest that substitution of W48 with phenylalanine impairs the pathway through which the extra electron is normally transferred. As a result, the two-electron-oxidized diiron species, designated as $(Fe_2O_2)^{4+}$, which in wild-type R2 would oxidize W48 to form **X** and the W48$^{+\bullet}$, instead oxidizes Y122 to form the **X**-Y$^\bullet$. Most of the Y122$^\bullet$ that forms as part of the **X**-Y$^\bullet$ subsequently decays. Decay of the Y122$^\bullet$ probably results from further reaction with the adjacent **X**, as indicated by the formation of altered diiron(III) products and by the ability of the strong reductant, dithionite, to "rescue" the Y122$^\bullet$ from decay by reducing **X** to form the normal μ-oxo diiron(III) cluster.

The preceding paper presents evidence that a transient tryptophan cation radical (W$^{+\bullet}$) forms upon reaction of O_2 with the diiron(II) cluster in protein R2 of *E. coli* class I ribonucleotide reductase (RNR).[1,2] The demonstration that this radical forms rapidly in a second-order reaction between the reactive Fe(II)-R2 complex and O_2 and is efficiently reduced by Fe(II)$_{aq}$, 2-mercaptoethanol, and ascorbate implicates a tryptophan-mediated electron-shuttling mechanism for transfer of the extra electron that is required for formation of the formally Fe(IV)-Fe(III) intermediate, cluster **X**, on the reaction pathway that leads to the tyrosyl radical/μ-oxo-diiron(III) cofactor of catalytically active RNR. A hydrogen-bonded network comprising the near surface residue W48, the second sphere residue D237, and the Fe1 ligand H118 was previously noted by Nordlund and coworkers,[3] who also recognized the similarity of this network to one found in cytochrome *c* peroxidase from yeast.[4] The cognate tryptophan residue in cytochrome *c* peroxidase (W191) is oxidized to a cation radical in formation of its compound I (compound ES) intermediate by heterolysis of a hydroperoxo-iron(III)-heme precursor.[5−11] As we previously noted,[12] this structural and apparent functional analogy marks W48 as the

* To whom correspondence should be addressed.
[§] Department of Physics, Emory University.
[†] Penn State University.
[⊥] Departments of Biochemistry and Chemistry, Emory University.
[‡] Current address: Altera Corporation, 101 Innovation Drive, San Jose, CA 95134.

(1) Baldwin, J.; Krebs, C.; Ley, B. A.; Edmondson, D. E.; Huynh, B. H.; Bollinger, J. M., Jr. *J. Am. Chem. Soc.* **2000**, *122*, 12195−12206.

(2) Abbreviations used: W48$^{+\bullet}$ (W$^{+\bullet}$), tryptophan cation radical formed from W48; R2, R2 subunit of *Escherichia coli* ribonucleotide reductase; **X**, the formally Fe(III)Fe(IV) cluster that accumulates during oxygen activation by R2; wt, wild-type; Y122$^\bullet$, the tyrosyl radical in R2 formed by the one-electron oxidation of residue Y122; **X**-Y$^\bullet$, intermediate containing both **X** and Y122$^\bullet$; equiv, equivalents.

(3) Nordlund, P.; Sjöberg, B.-M.; Eklund, H. *Nature* **1990**, *345*, 593−598.

(4) Finzel, B. C.; Poulos, T. L.; Kraut, J. *J. Biol. Chem.* **1984**, *259*, 13027−13036.

(5) Houseman, A. L. P.; Doan, P. E.; Goodin, D. B.; Hoffman, D. M. *Biochemistry* **1993**, *32*, 4430−4443.

(6) Fishel, L. A.; Farnum, M. F.; Mauro, J. M.; Miller, M. A.; Kraut, J.; Liu, Y.; Tan, X.; Scholes, C. P. *Biochemistry* **1991**, *30*, 1986−1996.

(7) Goodin, D. B.; McRee, D. E. *Biochemistry* **1993**, *32*, 3313−3324.

(8) McRee, D. E.; Jensen, G. M.; Fitzgerald, M. M.; Siegel, H. A.; Goodin, D. B. *Proc. Natl. Acad. Soc. U.S.A.* **1994**, *91*, 12847−12851.

10.1021/ja001279m CCC: $19.00
Published on Web 11/22/2000

Scheme 1. Proposed Mechanism of O_2 Activation in Fe(II)-R2-W48F[a]

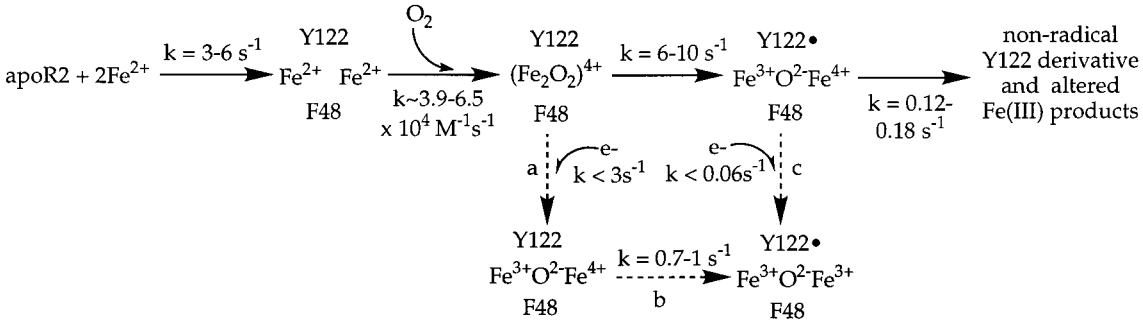

[a] The broken arrows associated with steps a−c are intended to convey that it is not clear whether steps a and b, or step c (or some combination of a + b and c) gives rise to the ∼0.25 equiv of Y122• that does not decay. Associated with this ambiguity, the rate constants describing the second and third steps in the primary pathway (along the top) are constrained only within the range given. For example, k_{obs} for the decay phase of Y122• reflects the sum of the rate constant for step c and the rate constant for the third step of the primary pathway, decay of the **X**-Y• species to nonradical products. If it is assumed that step c occurs with a rate constant of 0.06 s^{-1}, then *k* for the third step of the primary pathway is 0.12 s^{-1}.

most likely candidate for the residue that undergoes transient oxidation to shuttle the extra electron. In this work, we have tested this hypothesis by replacing W48 with phenylalanine, which we expected to be incapable of functioning in an electron shuttling capacity. Characterization of O_2 activation in R2-W48F has provided two lines of evidence to corroborate the involvement of this residue in the electron transfer that takes place in the reaction of the wild-type protein (R2-wt). The first line comprises chemical, kinetic, and spectroscopic data that are interpreted according to the mechanistic hypothesis shown in Scheme 1. A two-electron-oxidized intermediate, designated as $(Fe_2O_2)^{4+}$, which does not accumulate in the reaction of the wild-type protein (presumably because of its rapid reduction by W48),[1] accumulates with a rate that is dependent on the concentration of O_2. In the absence of its normal co-reactant, W48, this intermediate oxidizes Y122 directly with a rate constant that is 10-fold greater than that for oxidation of Y122 by **X**. This step forms a diradical species that contains both **X** and Y122• (designated as **X**-Y•). Presumably as a consequence of the proximity of **X** and Y122• and the inability of the protein to support reduction of either, the **X**-Y• species is unstable. Thus, the majority of the Y122• decays along with **X** in an as-yet-uncharacterized reaction that also produces altered diiron(III) products. A sub-stoichiometric quantity (∼0.25 equiv) of Y122• does not decay and is as stable as the Y122• produced in R2-wt. The failure of this sub-stoichiometric Y122• to decay with the majority is attributed to inefficient transfer ("leaking") of an electron to the cluster in competition with the primary mechanistic pathway. This electron may leak either to the $(Fe_2O_2)^{4+}$ species to give an intermediate containing only **X**, which subsequently converts to the normal Y122•/μ-oxo-diiron-(III) product, or to **X** of the **X**-Y• species to give the same product directly.

The second line of evidence consists of spectroscopic and theoretical characterization of the **X**-Y• species. Dipolar and weak exchange coupling between **X** and Y122• make the EPR spectrum of the diradical species broader than that of either of its constituent radicals in magnetic isolation. This weak spin−spin interaction gives rise to diamagnetic electronic states that are populated at 4.2 K in the absence of a strong magnetic field, resulting in the appearance of quadrupole doublet components in the weak-field Mössbauer spectrum that are not observed in the corresponding spectrum of magnetically isolated **X**. Application of a strong magnetic field increases the energy separation between the diamagnetic ($S = 0$) and the paramagnetic ($S = 1$) state and depopulates the former, rendering the Mössbauer spectrum of **X** in the **X**-Y• species nearly indistinguishable from that of magnetically isolated **X**. A theoretical analysis, which makes use of the previously determined magnetic parameters of the individual radical species[13−18] to provide constraints for a multiparameter simulation of the spectral data, provides insight into the nature of the spin coupling and the spatial relationship between the paramagnets. Consistent with the prediction from the crystal structure of the protein,[3] the two radical constituents are estimated to be ∼8 Å apart (when each is considered as a point dipole). This detailed characterization thus provides convincing evidence for the most important aspect of the mechanism of Scheme 1: the rapid and nearly quantitative formation of the **X**-Y• species as a consequence of the defect in electron injection in the W48-substituted variant.

Materials and Methods

Preparation and Quantitation of Apo R2-W48F. Mutagenesis of codon 48 in the *nrdB* gene to an F codon in the construction of the expression vector, pR2-W48F/F208Y, has been described.[19] Codon 208 was subsequently reverted back to Y to give pR2-W48F by replacement of the 471 basepair *Aat*II-*Hind*III restriction fragment of pR2-W48F/F208Y with the corresponding fragment from the previously described vector, pR2wt-*Hind*III. The sequence of the entire coding region of pR2-W48F was verified. Growth of *E. coli* strain BL21(DE3) (Novagen) transformed with pR2-W48F and purification of apo R2-W48F were

(9) Sivaraja, M.; Goodin, D. B.; Smith, M.; Hoffman, B. M. *Science* **1989**, *245*, 738−740.
(10) Erman, J. E.; Vitello, L. B.; Mauro, J. M.; Kraut, J. *Biochemistry* **1989**, *28*, 7992−7995.
(11) Huyett, J. E.; Doan, P. E.; Gurbiel, R.; Houseman, A. L.; Sivaraja, M.; Goodin, D. B.; Hoffman, B. M. *J. Am. Chem. Soc.* **1995**, *117*, 9033−9041.
(12) Bollinger, J. M., Jr.; Tong, W. H.; Ravi, N.; Huynh, B. H.; Edmondson, D. E.; Stubbe, J. *J. Am. Chem. Soc.* **1994**, *116*, 8024−8032.
(13) Burdi, D.; Sturgeon, B. E.; Tong, W. H.; Stubbe, J.; Hoffman, B. M. *J. Am. Chem. Soc.* **1996**, *118*, 281−282.
(14) Ravi, N.; Bollinger, J. M., Jr.; Huynh, B. H.; Edmondson, D. E.; Stubbe, J. *J. Am. Chem. Soc.* **1994**, *116*, 8007−8014.
(15) Riggs-Gelasco, P. J.; Shu, L.; Chen, S.; Burdi, D.; Huynh, B. H.; Que, L., Jr.; Stubbe, J. *J. Am. Chem. Soc.* **1998**, *120*, 849−860.
(16) Sturgeon, B. E.; Burdi, D.; Chen, S.; Huynh, B. H.; Edmondson, D. E.; Stubbe, J.; Hoffman, B. M. *J. Am. Chem. Soc.* **1996**, *118*, 7551−7557.
(17) Gerfen, G. J.; Bellew, B. F.; Un, S.; Bollinger, J. M., Jr.; Stubbe, J.; Griffin, R. G.; Singel, D. J. *J. Am. Chem. Soc.* **1993**, *115*, 6420−6421.
(18) Bender, C. J.; Sahlin, M.; Babcock, G. T.; Barry, B. A.; Chandrashekar, T. K.; Salowe, S. P.; Stubbe, J.; Lindström, B.; Petersson, L.; Ehrenberg, A.; Sjöberg, B.-M. *J. Am. Chem. Soc.* **1989**, *111*, 8076−8083.
(19) Parkin, S. E.; Chen, S.; Ley, B. A.; Mangravite, L.; Edmondson, D. E.; Huynh, B. H.; Bollinger, J. M., Jr. *Biochemistry* **1998**, *37*, 1124−1130.

initially accomplished as previously described.[19,20] All experiments except those depicted in Figures 1, 4A,C, and 6 were carried out with protein that had been prepared in this manner. In the course of this study, several modifications of these procedures were implemented in response to insight obtained in a parallel study on site-directed R2 variants with certain other amino acids (A, G, Q, L) at position 48. The inclusion of 10% (weight/volume) glycerol in the culture medium and the use of a simplified purification process that also includes 10% glycerol in the buffers were found to significantly augment both the yield and quality (purity and quantity of Fe(II) incorporated) of several of the W48X variants. It seems that the glycerol has the dual effects of facilitating folding of otherwise inefficiently folded variants and of enhancing the stability of less stable variants.[21−23] These modifications have been incorporated into our standard protocol. For the specific case of R2-W48F, the modifications do not significantly affect yield, purity, or "activity". Therefore, the modified procedure will be described in detail elsewhere.[24] Here we simply note that protein prepared by the new procedure was used for the experiments of Figures 1, 4A,C, and 6.

The modified fermentation protocol described below was found in all cases to improve the yield of cell mass. It also necessitated a higher concentration of phenanthroline in the chelation step that precedes induction of protein synthesis, presumably as a consequence of a greater iron content in the enriched medium. One liter cultures in a medium containing 35 g/L tryptone, 20 g/L yeast extract, 5 g/L sodium chloride, 10% (weight/volume) glycerol, 35 μL/L Antifoam A (Sigma product no. A-5758), and 150 mg/L ampicillin were shaken vigorously at 37 °C in 2.8 L baffled Fernbach flasks. The cultures were allowed to reach $OD_{600} = 1$, and 1,10-phenanthroline was then added to 0.5 mM. Fifteen minutes after this addition, isopropylthiogalactopyranoside (IPTG) was added to a concentration of 0.2 mM to induce synthesis of R2-W48F. The cultures were shaken for an additional 3 h and then were chilled on ice for several minutes prior to being harvested by centrifugation for 10 min at 4500 × G. The pelleted cells were washed by resuspension in a pre-chilled solution (3.3 mL per g of cell paste) of 25 mM Tris·HCl (pH 7.4), 0.1 M NaCl, 0.04 M KCl, and 10% glycerol followed by centrifugation as before. The cell paste was then frozen in liquid N_2 for storage. A typical yield was 5 g of wet cell paste per liter of culture.

The concentration of apo R2-W48F was determined spectrophotometrically by using the molar absorptivity at 280 nm ($\epsilon_{280} = 109$ mM^{-1} cm^{-1}), which was calculated according to the method of Gill and von Hippel.[25]

Titration of Apo R2-W48F with Fe(II). Serial additions of a 10 mM stock solution of ferrous ammonium sulfate in 5 mN H_2SO_4 were made at ambient temperature to a 350 μL aliquot of 0.1−0.2 mM apo R2-W48F in buffer B containing 2.5 mM sodium ascorbate. In some cases, 10% glycerol was also present in the buffer (it had no effect). At the beginning of the experiment and after each addition of Fe(II), the absorption spectrum of the sample was recorded every 30 s until the value of $A_{411} - (A_{405} + A_{417})/2$ no longer increased with time. When $A_{411} - (A_{405} + A_{417})/2$ no longer increased upon further addition of Fe(II), three more additions were made to facilitate data analysis.

Preparation of Product Samples by Reaction of Fe(II)-R2-W48F with O_2 (±Dithionite) or H_2O_2. The Fe(II)-R2-W48F complex was prepared (with or without 4 mM sodium dithionite) as described previously.[19] Reaction of the complex with O_2 was carried out (as previously described[19]) at 5 ± 3 °C by forceful injection via a gastight syringe of 200−250 μL of O_2-saturated 100 mM Na−Hepes (pH 7.6) into a septum-sealed microcentrifuge tube containing an equivalent volume of the Fe(II)-R2-W48F solution, which was continuously stirred by gentle vortexing during the addition. In preparation of the Mössbauer samples, 3 such samples with final protein concentrations of 0.12 mM were combined and the volume of the pool was reduced to give a protein concentration of 0.38 mM. Reaction of the complex with H_2O_2 was accomplished in the anaerobic chamber (at 24 °C) by addition of a freshly prepared 0.2 M stock solution in water to a final concentration of 2 mM. For each of the above samples, an absorption spectrum was recorded on a Hewlett-Packard 8453 Diode Array spectrometer immediately after the samples were prepared.

Stopped-Flow Spectrophotometry. Spectrophotometric monitoring of the reaction of apo R2-W48F with Fe(II) and O_2 was carried out with a Hi-Tech SFA-20 rapid mixing accessory and the aforementioned Hewlett-Packard spectrometer. Both components were actuated manually, with data acquisition being initiated immediately before mixing. Stopped-flow experiments in which the Fe(II)-R2-W48F complex was mixed with O_2 were carried out as described in the preceding paper[1] (with the KinTek apparatus housed in the anaerobic chamber). Time-dependent spectra were constructed from traces taken at individual wavelengths. With the slit widths that were employed on the Gilford Model 240 light source (0.4 mm, except for the experiment of Figure 4B, when they were 0.5 mm), the spectral resolution was somewhat less than for the Hewlett-Packard instrument. This fact accounts for the somewhat broader appearance of the 411 nm peak of the tyrosyl radical in Figure 4B than in Figure 4A and the smaller value of $\epsilon_{411-(405+417)/2}$ on the KinTek instrument than on the Hewlett-Packard instrument (vide infra). Specific reaction conditions for each experiment are given in the appropriate figure legend.

Determination of $\epsilon_{411-(405+417)/2}$ for Y122• in R2-W48F. We verified that the effective molar absorptivity ($\epsilon_{411-(405+417)/2}$) for the "411-nm peak height" treatment that we have used to quantify Y122• spectrophotometrically is the same in R2-W48F as in R2-wt. A series of 12 samples of R2-W48F were prepared with [Y122•] in the range of 0−50 μM. Samples were prepared both with and without dithionite. The absorption spectrum of each sample was acquired on the Hewlett-Packard spectrometer and the concentration of Y122• was then determined by EPR spectroscopy, as previously described.[26] A plot of $A_{411} - (A_{405} + A_{417})/2$ versus [Y122•] was quite linear, intercepting the origin and having a slope ($\epsilon_{411-(405+417)/2}$) of $(2.15 \pm 0.05) \times 10^3$ M^{-1} cm^{-1}, which is identical with the value determined for R2-wt. Comparison of $A_{411} - (A_{405} + A_{417})/2$ on the Hewlett-Packard instrument to that on the KinTek instrument (under the conditions used for the stopped-flow experiments) allowed $\epsilon_{411-(405+417)/2} = (1.5 \pm 0.1) \times 10^3$ M^{-1} cm^{-1} to be calculated for the latter.

Freeze-Quench EPR and Mössbauer Experiments. EPR and Mössbauer samples freeze-quenched at various reaction times were prepared as previously described.[14] The protein concentration was 0.5 mM and the Fe(II)/R2-W48F ratio was 2.5−3.0. EPR spectra were acquired on the Bruker ER 200D-SRC spectrometer described in the preceding paper. Spectrometer settings are given in the figure legends. The weak-field and strong-field Mössbauer spectrometers have been described.[14] The EPR spectral simulation was performed with the programs SIM and SIMSPC written by Høgni Weihe, University of Copenhagen.[27−29] The 32 × 32 matrix of the spin Hamiltonian (eq 1) required for the EPR simulation was set up by the standard method. Analysis of the Mössbauer data was performed with the program WMOSS (WEB Research).

Chemical Quench Experiments to Monitor Kinetics of Fe(II) Oxidation. A KinTek Corporation (State College, PA) Model RQF3 quenched-flow apparatus housed in the anaerobic chamber was maintained at 5 °C by a circulating water bath. The sample loops of this instrument were loaded with 13.7 μL each of 0.5 mM Fe(II)-R2-W48F (4 equiv Fe) and O_2-saturated buffer B. These solutions were driven to mix by flow of buffer (100 mM HEPES, pH 7.6) from the drive syringes and were passed through aging loops of variable volume (to give variable reaction time). Upon exiting the aging loop, the ~27.4

(20) Moënne-Loccoz, P.; Baldwin, J.; Ley, B. A.; Loehr, T. M.; Bollinger, J. M., Jr. *Biochemistry* **1998**, *37*, 14659−14663.
(21) The ability of glycerol to function as a "chemical chaperone" was previously noted by Massey and co-workers (see refs 22 and 23).
(22) Raibekas, A. A.; Massey, V. *Proc. Natl. Acad. Soc. U.S.A.* **1996**, *93*, 7546−7551.
(23) Raibekas, A. A.; Massey, V. *J. Biol. Chem.* **1997**, *272*, 22248−22252.
(24) Kelch, B. A.; Pathickal, B. A.; Baldwin, J.; Ley, B. A.; Krebs, C.; Huynh, B. H.; Bollinger, J. M., Jr., unpublished results.
(25) Gill, S. C.; von Hippel, P. H. *Anal. Biochem.* **1989**, *182*, 319−326.
(26) Bollinger, J. M., Jr.; Tong, W. H.; Ravi, N.; Huynh, B. H.; Edmondson, D. E.; Stubbe, J. *J. Am. Chem. Soc.* **1994**, *116*, 8015−8023.
(27) Glerup, J.; Weihe, H. *Acta Chem. Scand.* **1991**, *45*, 444−448.
(28) Jacobsen, C. J. H.; Pedersen, E.; Villadsen, J.; Weihe, H. *Inorg. Chem.* **1993**, *32*, 2.
(29) Glerup, J.; Weihe, H. *Inorg. Chem.* **1997**, *36*, 2816−2819.

μL "slug" of reaction solution pushed from behind by buffer was mixed with 0.5 equivalent volumes of 0.5 N H_2SO_4. This chemical quench stops the reaction and stabilizes unreacted Fe(II) against autoxidation. The procedure used yielded samples of approximately 130 μL. A zero-time sample was prepared by manual addition of 13.7 μL of the protein reactant directly to an O_2-free solution prepared by mixing 80 μL of buffer B and 40 μL of 0.5 N H_2SO_4. Reaction samples were removed from the anaerobic chamber and centrifuged to pellet the denatured protein. A 50-μL aliquot of each sample was added to a solution consisting of 260 μL of H_2O, 10 μL of a saturated solution of ammonium acetate, and 10 μL of 10 mM ferrozine. A second 50-μL aliquot of each was added to an equivalent solution containing 2.5 mM ascorbate. The former served to quantify (by comparison of its A_{562} to a standard curve) unreacted Fe(II), whereas the latter allowed quantitation of the extent of recovery of the Fe in the reactant (because ascorbate reduced any Fe(III) to allow its detection). A control experiment confirmed that added Fe(III) (from a solution of ferric ammonium sulfate dissolved in 0.17 N H_2SO_4) is quantitatively detected by ferrozine in the presence of ascorbate but is not detected in the absence of the reductant. Thus, detection in the presence of ascorbate provided, in essence, an internal standard. Each timepoint in a given experiment was performed in duplicate, and the results of four experiments were averaged in the construction of Figure 14.

Results and Discussion

Preparation of Active Apo R2-W48F. Preparation of "active" (with respect to Fe(II) binding and O_2 activation) apo R2-W48F for mechanistic characterization of O_2 activation and evaluation of the proposed electron-shuttling role of W48 in wild-type R2 required prevention of prior exposure of the variant protein to Fe(II) and O_2 during its expression and purification. This was achieved by our published procedure of chelating available Fe(II) by addition of phenathroline to the culture immediately prior to induction of expression and at early steps in the purification.[19] Protein prepared by more standard procedures (with no steps taken to prevent exposure to Fe) emerged from the purification with much less than its theoretical complement of Fe (0.65 equiv in each of two trials), but did not take up added Fe(II) nor activate O_2. To demonstrate that this inactivity could result from modification of the protein as a result of its prior exposure to Fe(II) and O_2, we reacted the *active* protein with excess Fe(II) and O_2, reductively removed the bound Fe(III) from the product, and attempted to react the protein a second time. The "pre-reacted" apo R2-W48F was found to take up, on average, only 56% as much Fe(II) (range of 34−71% in four separate experiments) and to produce only 44% as much stable Y122$^\bullet$ (range of 27−55%) as the previously unreacted apo protein. By contrast, pre-reacted apo R2-wt produced the same quantity of Y122$^\bullet$ (1.2 ± 0.1 equiv) as the unreacted apo protein. Apparently, a single round of O_2 activation in R2-W48F leads to loss of approximately one-half of its "activity". The nearly complete inactivity of R2-W48F produced in the absence of phenanthroline probably results from multiple cycles of O_2 activation followed by in situ reduction of the Fe(III) product. (An enzymatic system that is capable of effecting this reduction has been identified and partially characterized.[30]) The inactivation of R2-W48F accompanying its O_2 reaction is consistent with the proposed role of W48 in control of the reaction. Procedural details for these experiments are provided in the Supporting Information.

Active apo R2-W48F prepared *with* Fe(II) chelation was found to take up 2.5−3.0 equiv of Fe(II) in the presence of O_2, as determined by spectrophotometrically monitored titrations (Figure 1) in which completion was deduced from plots of the intensity of the 411 nm absorption feature of Y122$^\bullet$ versus Fe/R2 (inset to Figure 1). That the values from these titrations accurately reflect the quantity of Fe(II) taken up by the protein was corroborated (in two separate experiments) by subsequent purification of the fully reacted protein by anion exchange chromatography and determination of the quantity of Fe bound by a denaturing colorimetric assay, which has been described.[31]

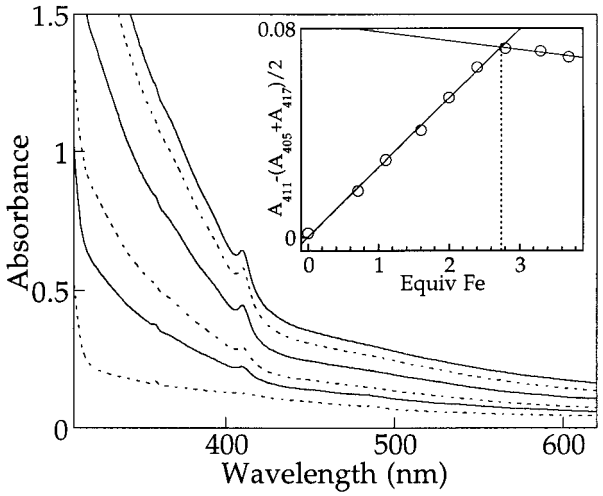

Figure 1. Spectrophotometrically monitored titration of apo R2-W48F with Fe(II) in the presence of O_2. The procedure is described in the Materials and Methods section. The spectra shown were recorded after addition of (from bottom to top) 0 (dotted trace), 0.71 (solid trace), 1.1 (dotted trace), 2.0 (solid trace), 2.8 (dotted trace), and 3.7 equiv (solid trace) of Fe(II). The inset is a plot of the 411 nm peak height as a function of the number of equiv of Fe(II) added, from which the equivalence point was determined. The initial protein concentration was 0.20 mM.

Altered Products of O_2 Activation in R2-W48F. Although this "active" apo R2-W48F incorporates 2.5−3.0 equiv of Fe(II), the 411-nm peak height ($A_{411} - (A_{405} + A_{417}/2)$ at completion indicates that much less Y122$^\bullet$ is formed than in R2-wt. Quantitation by EPR indicates that only 0.25 ± 0.03 equiv of Y122$^\bullet$ is formed when the reaction is carried out at 5 °C, which gives an Fe(II)/Y122$^\bullet$ stoichiometry of 10−12. By contrast, the Fe(II)/Y122$^\bullet$ stoichiometry for R2-wt is ∼3.3. Thus, a much smaller fraction of reaction events results in formation of stable Y122$^\bullet$ in R2-W48F. The weak-field (50 mT) Mössbauer spectrum of the fully reacted protein (Figure 2, spectrum A) exhibits features that may be ascribed to the μ-oxo-diiron(III) cluster (solid line plotted above the data). From a detailed analysis of the spectrum,[32] it was deduced that these features contribute 23 ± 4% of the total iron absorption, which corresponds to 0.58 ± 0.1 equiv of Fe or 0.29 ± 0.05 equiv of μ-oxo-diiron(III) cluster. This value is similar to the quantity of Y122$^\bullet$ determined by EPR. The majority of the absorption area that does not arise from the μ-oxo-diiron(III) cluster is attributable to at least three other Fe(III) species, of which two are diamagnetic and are probably antiferromagnetically coupled dinuclear clusters and the third is paramagnetic.[32] For the purposes of this paper, the identities of these altered products are unimportant. The relevant point is that similar quantities of the two normal products (Y122$^\bullet$ and μ-oxo-diiron(III) cluster) form, suggesting that they are formed in the same reaction events. Conversely, those events that do not produce stable Y122$^\bullet$ are apparently associated with formation of altered iron(III) products.

(30) Fontecave, M.; Nordlund, P.; Eklund, H.; Reichard, P. *Adv. Enzymol. Rel. Areas Mol. Biol.* **1992**, *65*, 147−183.

(31) Bollinger, J. M., Jr. Ph.D. Thesis, Massachusetts Institute of Technology, 1993.

(32) Chen, S. Ph.D. Thesis, Emory University, 1997.

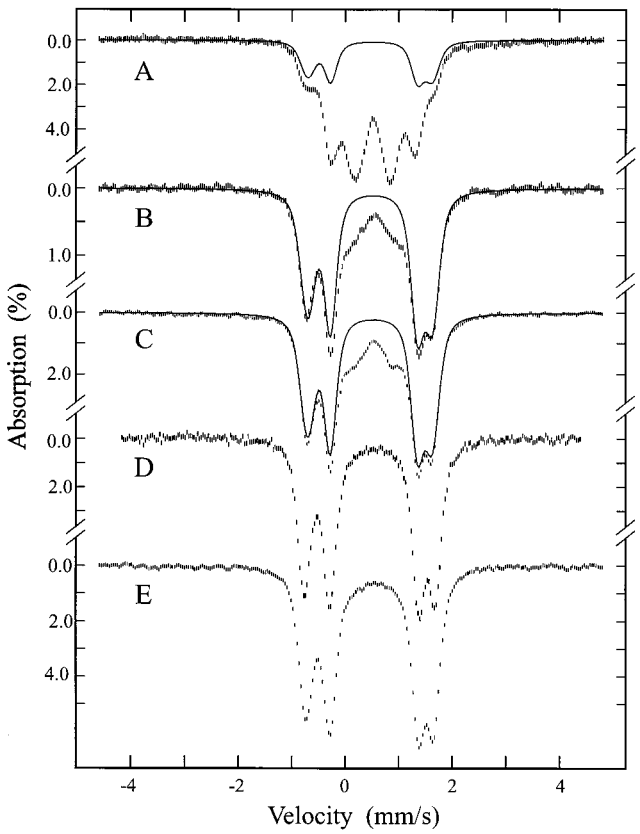

Figure 2. Mössbauer spectra of the products of the reactions of (A) Fe(II)-R2-W48F with O_2 in the absence of dithionite, (B) Fe(II)-R2-W48F with O_2 in the presence of 2 mM dithionite, (C) Fe(II)-R2-W48F with 2 mM H_2O_2, (D) Fe(II)-R2-wt with O_2, and (E) Fe(II)-R2-wt with 2 mM H_2O_2. The data are recorded at 4.2 K with a parallel applied field of 50 mT. The solid lines are theoretical simulations of the μ-oxo diiron(III) cluster scaled to 23%, 80%, and 77% of the integrated intensities of the spectra A, B, and C, respectively. The observed parameters ($\Delta E_Q(1) = 1.63 \pm 0.04$ mm/s and $\delta(1) = 0.54 \pm 0.02$ mm/s; $\Delta E_Q(2) = 2.34 \pm 0.04$ mm/s and $\delta(2) = 0.46 \pm 0.02$ mm/s) for the μ-oxo-diiron(III) cluster in R2-W48F are practically identical with those for the R2-wt cluster, except that the latter exhibits slightly narrower lines (compare spectrum D with the solid lines).

Evidence that the Formation of Altered Products Is a Consequence of Defective Electron Transfer. It is conceivable that the low yield of Y122• and the production of altered iron(III) products in R2-W48F might be consequences of a general structural defect resulting from the nonisosteric substitution. Two lines of evidence contradict this interpretation and indicate that these outcomes are specific hallmarks of blocked electron injection. First, much greater quantities of the normal μ-oxo-diiron(III) cluster and tyrosyl radical can be produced when the reaction is carried out in the presence of the strong reductant, dithionite. The Mössbauer spectrum of a sample prepared by reacting the Fe(II)-R2-W48F complex with O_2 in the presence of 2 mM dithionite (Figure 2, spectrum B) shows that 80 $\pm$ 4% of the 2.7 equiv of Fe(II) that was present in the reactant has been converted to the μ-oxo-diiron(III) cluster (solid line plotted over the data). This value corresponds to a stoichiometry of 1.08 $\pm$ 0.06 μ-oxo-diiron(III) cluster/R2-W48F, which is three times the quantity produced in the absence of dithionite and more than two-thirds the quantity produced in R2-wt. Samples prepared in this manner also have 0.65 $\pm$ 0.05 equiv of Y122• (Figure 3, solid line), which is 2.6 times as much as is produced in the absence of the reductant (Figure 3, dotted line). It is possible that even greater quantities of the normal products would be formed if a higher concentration of dithionite could be used, but such attempts are thwarted by the fact that dithionite (or, more precisely, the SO_2 radical anion produced by homolytic dissociation of the parent species) reacts rapidly with O_2 and thereby inhibits the R2 reaction at concentrations in excess of 2 mM. Nevertheless, it is clear that greater quantities of the normal products are formed if the extra electron is "forced" into the active site by dithionite. *Once formed, these products are as stable as in R2-wt.*

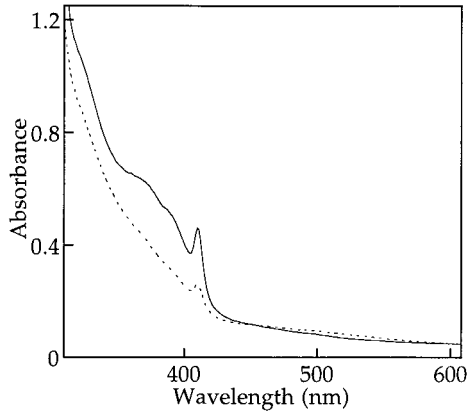

Figure 3. Light absorption spectra of the products of the reaction of the Fe(II)-R2-W48F complex (2.7 equiv of Fe) with O_2 in the absence (dotted trace) and in the presence (solid trace) of 2 mM sodium dithionite. The preparation of these samples is described in the Materials and Methods section. The final protein concentration was 0.11 mM.

The second line of evidence against a general structural defect comes from reaction of the Fe(II)-R2-W48F complex with H_2O_2. Fontecave and co-workers reported that reaction of Fe(II)-R2-wt with H_2O_2 produces the μ-oxo-diiron(III) cluster but no Y122•.[33] Although they offered only the absorption spectrum of the product as evidence, their interpretation is entirely consistent with electron accounting: H_2O_2 is a two-electron oxidant, and its reaction with the two-electron-reduced diiron center is balanced for direct formation of the product cluster without additional oxidation products. We first verified the conclusion of Fontecave and co-workers with the wild-type protein. Indeed, the Mössbauer spectrum of the product of the reaction of Fe(II)-R2-wt with H_2O_2 (Figure 2, spectrum E) is virtually indistinguishable from that of the product of reaction of the complex with O_2 (Figure 2, spectrum D) and reflects the presence of 1.5 $\pm$ 0.15 equiv of μ-oxo-diiron(III) cluster. The same sample has $<$0.1 equiv of Y122•, which we attribute to prior reaction of the complex with contaminating O_2 instead of H_2O_2. Reaction of Fe(II)-R2-W48F (2.5 equiv of Fe(II)) with H_2O_2 also produces primarily (77 $\pm$ 4% or 0.96 $\pm$ 0.06 equiv) the μ-oxo-diiron(III) cluster (Figure 2, spectrum C). The spectrum of this sample is very similar to that of the product of reaction of Fe(II)-R2-W48F with O_2 in the presence of dithionite (Figure 2, spectrum B). The minority species appear on the basis of their Mössbauer spectra to be the same in these two samples, and may represent Fe(III) bound to protein that was previously oxidatively damaged (by reaction with Fe(II) and O_2) despite our attempts to prevent this. Nevertheless, the majority of the R2-W48F protein is clearly capable of forming and stabilizing both the μ-oxo-diiron(III) cluster and the tyrosyl radical, but these products predominate only under reaction conditions that relax the usual requirement for the protein to mediate the electron transfer step. These observations provide compelling argument that the W48F substitution causes a defect specifically in this step.

(33) Gerez, C.; Fontecave, M. *Biochemistry* **1992**, *31*, 780−786.

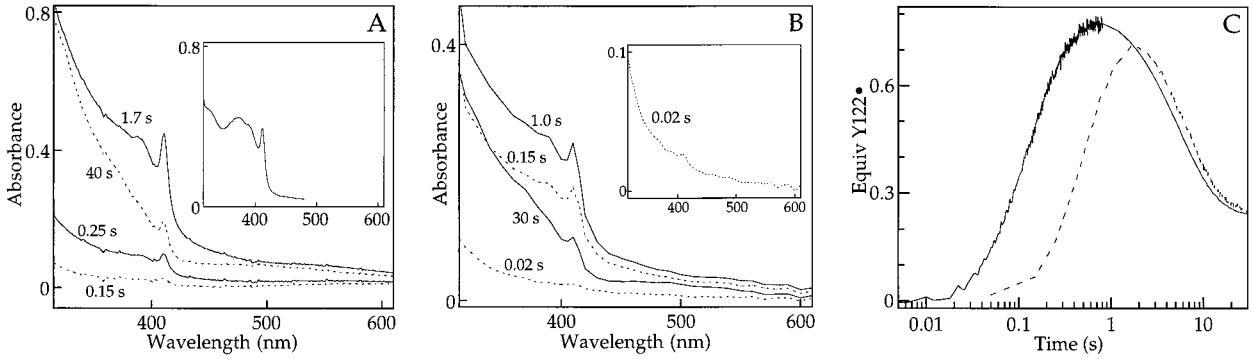

Figure 4. Timecourse of O_2 activation at 5 °C by R2-W48F monitored by stopped-flow absorption spectroscopy. (A) Spectra obtained after 1:1 mixing of apo R2-W48F in air-saturated buffer B containing 10% glycerol with 3.5 equiv of Fe(II) in O_2-saturated (at 25 °C) 5 mN H_2SO_4 also containing 10% glycerol. (It was verified that the presence of glycerol had no detectable effect on the reaction kinetics or outcome.) The final concentration of O_2 should have been 0.75 mM. The inset shows, for comparison, a superposition of the spectra of the μ-oxo-diiron(III) cluster and the tyrosyl radical at a 1:1 molar ratio. (B) Spectra reconstructed from single-wavelength kinetic traces obtained after 1:1 mixing of the preformed Fe(II)-R2-W48F complex (3.0 equiv Fe) in buffer B with O_2-saturated (at 25 °C) buffer B. The final [O_2] should have been 0.63 mM. Each spectrum represents the change in absorbance from the "deadtime" of the apparatus until the indicated time. The agreement of the spectra at completion in parts A and B confirms that little if any absorbance develops in the deadtime, and thus that the treatment is valid. The inset in part B is a "blow-up" of the 20 ms spectrum. In both parts A and B, the final protein concentration was 0.10 mM. (C) Timecourse of the 411-nm peak height for the reaction of part A (dotted trace) and a reaction similar to that of part B (solid trace). To obtain the solid trace, 0.41 mM Fe(II)-R2-W48F (3.0 equiv Fe) in buffer B containing 10% glycerol was mixed in a 1:2 volume ratio with 50% saturated (at 5 °C) buffer B containing 10% glycerol. The final [O_2] should have been 0.66 mM.

Timecourse of O_2 Activation in R2-W48F by Stopped-Flow Absorption Spectroscopy. Additional evidence for this conclusion and insight into the specific mechanistic consequences of defective electron transfer in R2-W48F are provided by a study of the kinetics of its O_2 reaction. Mixing at 5 °C of apo R2-W48F with excess Fe(II) and O_2 (Figure 4A) or of the preformed Fe(II)-R2-W48F complex with O_2 (Figure 4B) results in rapid development of the sharp 411-nm and broader 390-nm features of the tyrosyl radical. The time-dependent spectra and, more quantitatively, the timecourses of the 411-nm peak height ($A_{411} - (A_{405} + A_{417})/2$; Figure 4C) indicate that much more Y122• develops during the reaction than remains in the final product. With the reasonable assumption that $\epsilon_{411-(405+417)/2}$ of the Y122• is the same during the reaction as for the final product, it can be determined from the absorption data that as much as 0.76 equiv of Y122• forms and that 60−75% then decays slowly ($k_{obs} = 0.18 \pm 0.05\ s^{-1}$) relative to its formation. The maximum quantity to accumulate (range of 0.6−0.76 equiv in multiple experiments) is very similar to the quantity of stable Y122• formed in the presence of dithionite. These observations indicate that the low yield of Y122• results from decay of the radical rather than an outright failure of the species to form. It warrants emphasis that this decay cannot reflect an inherent instability of the product radical in the variant protein, since the 0.65 ± 0.05 equiv of Y122• made in the presence of dithionite is as stable as that in R2-wt. Rather, this decay must reflect production of the radical in an altered mechanistic context, in which it is subject to further reaction leading to its decay. The spectra at times near the maximum of Y122• concentration provide a clue as to this context: the 365-nm feature, which is characteristic of the product μ-oxo-diiron(III) cluster, is less apparent than would be expected in a 1:1 admixture of it and Y122• (compare the 1.7-s spectrum of Figure 4A to the inset of Figure 4A or to the solid trace in Figure 3). As is documented in subsequent sections by freeze-quench EPR and Mössbauer data, this observation is rationalized by the concomitant formation of Y122• and **X** and the fact that **X** exhibits only half the molar absorptivity at 365 nm of the μ-oxo-diiron(III) cluster.

Evidence for Accumulation of a Diiron(II)-O_2 Adduct. The kinetics of formation of Y122• under different reaction conditions provide additional mechanistic insight. The shorter lag phase and greater rate of formation for the reaction in which the preformed Fe(II)-R2-W48F complex is mixed with O_2 (Figure 4C) indicates that, as in the case of R2-wt, conversion of the apo protein into the reactive Fe(II)-protein complex rate-limits O_2 activation when apo R2-W48F is mixed with Fe(II) and O_2. Simulations of the kinetic data acquired by this reaction protocol suggest that formation of the reactive complex has an apparent first-order rate constant of 4.5 ± 1.5 s^{-1}, which is identical with that observed for R2-wt. The existence of a lag phase even when the complex has been preformed suggests that an adduct between Fe(II)-R2-W48F and O_2, designated as $(Fe_2O_2)^{4+}$, accumulates on the pathway to Y122•, as depicted in Scheme 2. (Because formation of Y122• is more than 40 times as rapid as its decay, it is possible to neglect the decay step in the following analysis without introducing significant error into the rate constants associated with the two steps required for its formation.) Fitting of the equation describing the concentration of Y122• in the mechanism of Scheme 2 to the early segments ($t = 0-0.7$ s) of the traces for the reaction of Fe(II)-R2-W48F with 1.3 mM O_2 (Figure 5, triangular data points and solid fit line) gives apparent first-order rate constants of 60 ± 9 s^{-1} for the first step and 8.7 ± 0.9 s^{-1} for the second step. (Each value of k_{obs} represents the mean and range obtained in four similar, independent experiments.) The accumulation of an $(Fe_2O_2)^{4+}$ intermediate on the pathway to Y122• is further corroborated by the dependence of the apparent first-order rate constant associated with the lag phase on the concentration of O_2 and the less pronounced dependence of the value of k_{obs} for the formation phase. For example, analysis of traces from reaction of the complex with 0.63 mM O_2 (Figure 5, circular points and solid fit line) gives rate constants of 38 ± 3 s^{-1} for the first

Scheme 2. Kinetic Scheme Used in Analysis of the Timecourses of Y122• Formation (as reported by the 411-nm peak height data) at Different O_2 Concentrations

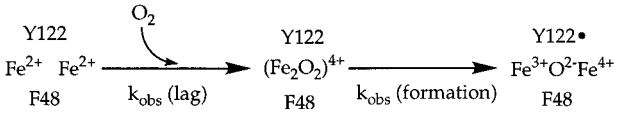

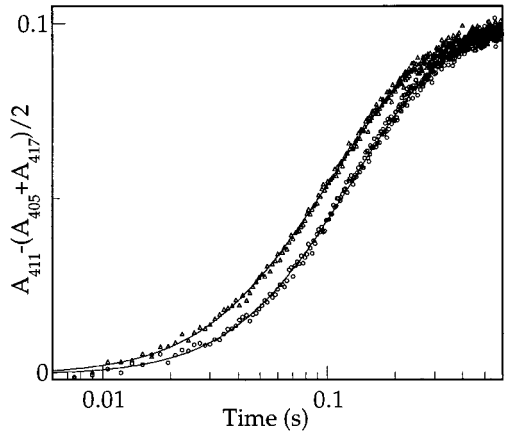

Figure 5. Dependence of the kinetics of Y122• formation on the concentration of O_2 during the reaction of Fe(II)-R2-W48F (3.2 equiv) with O_2. The Fe(II)-R2-W48F complex (0.50 mM initial concentration) in buffer B was mixed at 5 °C in a 1:2 volume ratio either with 50% O_2-saturated buffer B (circular points) or with 100% O_2-saturated buffer B (triangular points). The solid fit lines are the best fits for the equation describing [Y122•] as a function of time for the mechanism of Scheme 2.

step and 7.7 ± 0.5 s^{-1} for the second step. It is not clear whether the slight $[O_2]$ dependence consistently observed in k_{obs} for the formation phase is significant. However, the *reversible* formation of an $(Fe_2O_2)^{4+}$ adduct preceding Y122• could account both for this dependence and for the observation that formation of the intermediate apparently has an O_2 kinetic order of less than 1. Under the simpler assumption that this intermediate forms in an *irreversible* second-order reaction between Fe(II)-R2-W48F and O_2, the apparent first-order rate constants deduced for formation of the intermediate at the two different concentrations of O_2 would correspond to a second-order rate constant of $(5.2 \pm 1.3) \times 10^4$ M^{-1} s^{-1}. This is approximately 4-fold less than the rate constant for reaction of Fe(II)-R2-wt with O_2.[1]

The value of k_{obs} for formation of Y122• ($\sim 7-10$ s^{-1}) is 10-fold greater than the rate constant for its generation by **X** in R2-wt ($0.7-1$ s^{-1}).[26,34] This observation is reminiscent of the reaction of R2-wt under conditions of limiting reductant (i.e. limiting Fe(II) and no additional reductant).[12] As shown in the preceding paper, approximately half of the Y122• produced in this reaction forms in a fast phase with an associated rate constant of $5-7$ s^{-1}, and this fast phase can be attributed to generation of Y122• by the W^{+}•.[1] Similarly, the simplest explanation for the fast formation of Y122• in R2-W48F is that Y122• is generated by an intermediate other than **X**. It has previously been shown that the fast phase of Y122• formation in the limiting Fe(II) reaction of R2-wt is eliminated by inclusion of mM concentrations of ascorbate.[12] This slowing effect can be attributed to the efficient reduction of the W^{+}• by ascorbate, which ensures that all of the Y122• is generated more slowly by **X**.[1] In contrast to the R2-wt reaction and in agreement with the proposed incompetence of R2-W48F to mediate transfer of the extra electron, the presence of 1 mM ascorbate does not retard Y122• formation (Figure 6A) in the reaction of the variant protein. Thus, the inferred intermediate that generates Y122• rapidly in R2-W48F is not rapidly reduced by ascorbate, a characteristic that clearly distinguishes it from the W^{+}• in the R2-wt reaction.

On the basis of the preceding paper's assignment of the 560-nm absorption in the R2-wt reaction with limiting Fe(II) to a $W48^{+}$•,[1] one would predict that this absorption should be eliminated by the W48F substitution. Indeed, A_{560} has a greatly diminished maximum value and shows very different kinetic behavior in the reaction of the variant protein with O_2 (Figure 6B, circular points). The transient absorption that persists may be attributed entirely to **X** and Y122• on the basis of the molar absorptivities of these species at 560 nm (given in the preceding paper)[1] and the observation that the rate constants extracted by fitting the 560-nm data precisely match those from analysis of the timecourse of the 411-nm peak height ($A_{411} - (A_{405} + A_{417}/2)$), which reflects only the concentration of Y122•. Confirming that this weak transient absorption does not arise from the same species as in the reaction of R2-wt (the W^{+}•), the presence of 1 mM ascorbate, which almost completely suppresses the 560-nm transient in the R2-wt reaction,[12] has an insignificant effect on the A_{560}-versus-time trace for the R2-W48F reaction (Figure 6B, triangular points). Thus, the species responsible for the intense 560-nm absorption in the limiting Fe(II) reaction of R2-wt does not form under equivalent reaction conditions (or any other conditions that we have investigated) in R2-W48F. This observation provides strong support for the attribution of the 560-nm absorption in the R2-wt reaction to a $W48^{+}$•.

Reaction of Apo R2-W48F with Fe(II) (2.5 Fe/R2-W48F) and O_2 Monitored by Freeze-Quench EPR and Mössbauer Spectroscopies. The key feature of the mechanistic hypothesis of Scheme 1 is the concomitant rather than sequential formation of **X** and Y122•. Evidence for this feature is provided by (1) correlation of UV−visible absorption, Mössbauer, and EPR kinetic data, which show that **X** and Y122• form together and (2) the unique EPR and Mössbauer spectral features that result from the spin−spin coupling of **X** and Y122•. It has already been shown that the concentration of Y122• reaches its maximum at 1−2 s in the reaction of apo R2-W48F with Fe(II) and O_2 (Figure 4C, dashed line). The weak-field (50 mT) Mössbauer spectra of samples freeze-quenched during the Y122• formation phase (Figure 7, spectrum A) clearly exhibit the paramagnetic features of **X** (solid line plotted above the data). As documented in the following sections, quantitation of **X** from the absorption area of these features is complicated by coupling between **X** and Y122•, which gives rise to quadrupole doublet components, in addition to the usual paramagnetic features, in the weak-field spectrum of **X**. The contribution of these doublet components can, however, be completely converted to the paramagnetic features by application of a strong (8 T) magnetic field. This allows **X** to be quantified in each sample by analysis of the field dependence of its Mössbauer spectrum (see below and Figure 7B, solid line). The quantities of **X** so determined (Figure 8, squares) confirm that its formation coincides temporally with the formation of Y122• reported by the UV−visible absorption data. This correlation is consistent with their concomitant formation.

Characterization of the reaction by freeze-quench EPR spectroscopy (Figure 9) provides additional evidence for the concomitant formation of **X** and Y122•. As expected, the spectrum at completion (Figure 9, spectrum F) is that characteristic of Y122•, and its intensity reflects the presence of 0.25 $\pm$ 0.05 equiv of the product radical. Paradoxically, the spectra of samples freeze-quenched during the formation phase of **X** and Y122• (Figure 9, spectra A to D) appear not to reflect the presence of either species. As described in the following sections, this apparent paradox is resolved by the recognition that the broad $g = 2$ signal that dominates the spectra of these samples arises from a coupled diradical species that contains *both **X** and Y122•*. Coupling between the two $S = {}^1/_2$ constituents

(34) Bollinger, J. M., Jr.; Edmondson, D. E.; Huynh, B. H.; Filley, J.; Norton, J. R.; Stubbe, J. *Science* **1991**, *253*, 292−298.

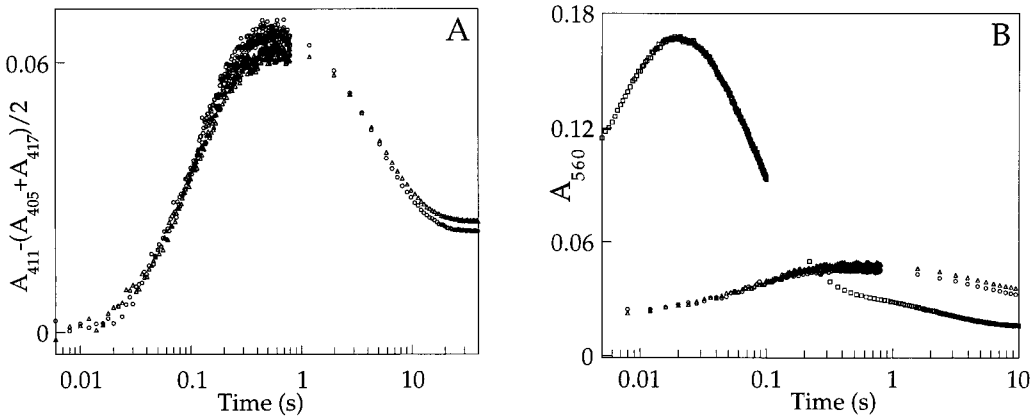

Figure 6. Insignificant effect of ascorbate on the kinetics of the 411-nm peak height and the absorbance at 560 nm in the reaction of Fe(II)-R2-W48F (3.0 equiv Fe) with O_2. The complex at an initial concentration of 0.35 mM in buffer B containing 10% glycerol was mixed at 5 °C in a 1:2 volume ratio with O_2-saturated buffer B containing 10% glycerol. (A) Timecourses of the 411-nm peak height for the reaction in the absence (circular points) and presence (triangular points) of 1 mM ascorbate. (B) Timecourses of A_{560} for the reaction in the absence (circular points) and presence (triangular points) of 1 mM ascorbate. In part B, the trace from Figure 1 of the preceding paper,[1] which is from an experiment in which the Fe(II)-R2-wt complex (3.2 equiv) was mixed in a 1:2 ratio with O_2-saturated buffer B, has been mathematically scaled for purposes of comparison to reflect a final protein concentration of 0.117 mM (square points).

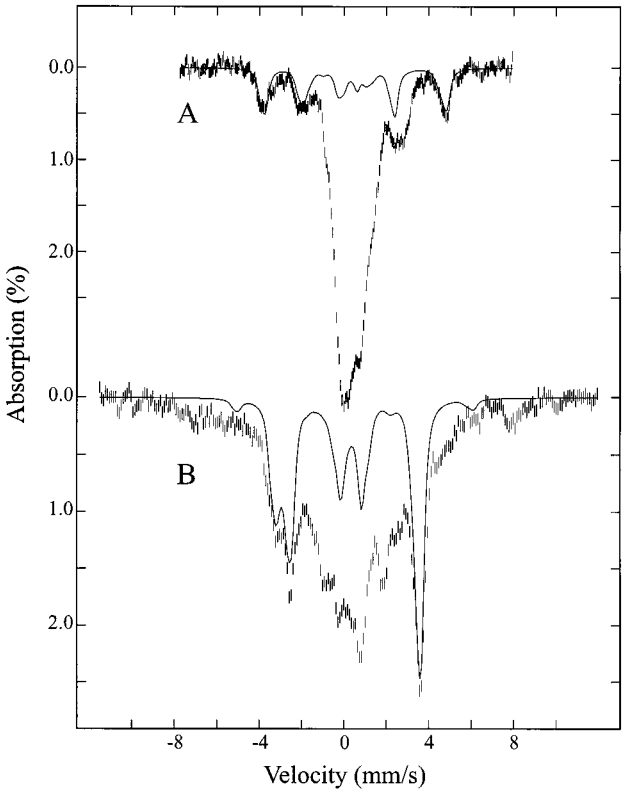

Figure 7. Mössbauer spectra of a sample freeze-quenched 1.7 s after 1:1 rapid mixing of an O_2-saturated solution of 1.0 mM apo R2-W48F with O_2-saturated Fe(II) (2.5 Fe/R2-W48F). The spectra were recorded at 4.2 K with a field of 50 mT (A) or 8 T (B) applied parallel to the γ-beam. The solid lines are theoretical simulations for a magnetically isolated **X** scaled to 20% (in A) and 38% (in B) of the integrated intensity of the experimental spectrum.

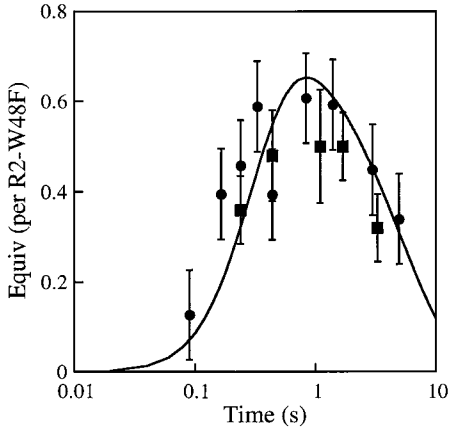

Figure 8. Quantities of **X** (squares) and **X**-Y$^\bullet$ species (circles) as functions of reaction time, as determined by analysis of the freeze-quenched Mössbauer and EPR spectra, respectively. The solid line is a theoretical simulation according to Scheme 1 that assumes effective rate constants of 6 s^{-1} for formation of the reactive Fe(II)-R2-W48F complex, 80 s^{-1} for formation of the $(Fe_2O_2)^{4+}$ species (the reaction solution was 100% O_2-saturated), 9 s^{-1} for formation of the **X**-Y$^\bullet$ species, and 0.18 s^{-1} for the sum of the two processes leading to decay of the **X**-Y$^\bullet$ species. The simulation also assumes that 0.7 equiv of R2-W48F reacts through this pathway.

renders their EPR spectra much broader than when they are magnetically isolated. All the spectra from a complete EPR timecourse for the reaction (including those shown in Figure 9) can be accounted for as superpositions of two component spectra, the spectrum of isolated Y122$^\bullet$ and a much broader spectrum that we attribute to the **X**-Y$^\bullet$ species (thicker line of Figure 10A). From the relative intensities of the two spectral components and the total spin concentration in each sample (the latter being determined from the double-integrated intensity of each spectrum), the quantities of **X**-Y$^\bullet$ and Y122$^\bullet$ present at each reaction time were estimated. For example, at 1.4 s, near the time of maximum concentration of Y122$^\bullet$, 0.59 ± 0.05 equiv of **X**-Y$^\bullet$ and 0.13 ± 0.03 equiv of isolated Y122$^\bullet$, or a total of 0.72 ± 0.06 equiv of Y122$^\bullet$, has accumulated. The latter value agrees well with that determined by stopped-flow absorption measurements (0.6−0.76 equiv). The quantities of the **X**-Y$^\bullet$ species determined by EPR (Figure 8 circles) also agree well with the quantities of **X** determined by Mössbauer (squares), and both of these are consistent with the timecourse of **X**-Y$^\bullet$ predicted by a simulation according to Scheme 1 (Figure 8, solid line). In this simulation, it was assumed that the 0.25 equiv of stable radical results from electron "leaking" to **X** in the **X**-Y$^\bullet$ species (step c in Scheme 1), and rate constants given in the figure legend were used. The acceptable agreement of the simulation with the data verifies that all three spectroscopic methods give consistent quantitation of the constituent radical

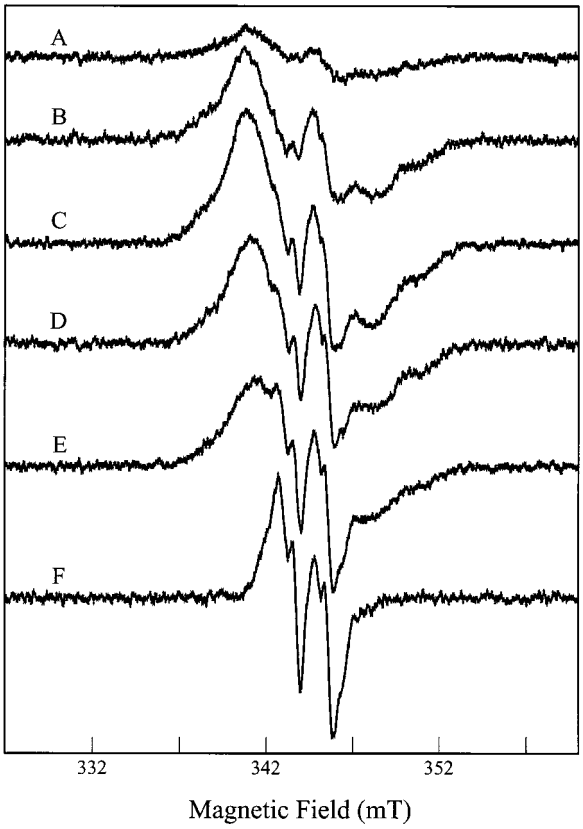

Figure 9. Time-dependent EPR spectra of the reaction of apo R2-W48F with O_2 and Fe(II) carried out as in Figure 7. The reaction was quenched at (A) 90 ms, (B) 440 ms, (C) 1.4 s, (D) 3 s, (E) 5 s, and (F) 60 s. The data were recorded at 20 K with a microwave power of 6.7 μW. Other instrumental settings were the following: microwave frequency, 9.65 GHz; modulation amplitude, 0.4 mT; modulation frequency, 100 kHz; and receiver gain, 8×10^4.

species, which in turn verifies the assumption made in analysis of the EPR data that the broad spectrum arises in equal parts from **X** and Y122•. The lack of resemblance of the broad spectrum to those of isolated **X** and Y122• is, then, compelling evidence for coupling of the two paramagnetic species. In the following section, we present detailed spectroscopic analysis and theoretical considerations that explain the unique spectroscopic features of the **X**-Y• species on the basis of this coupling.

Detailed Spectroscopic and Theoretical Characterization of the X-Y• Diradical Species. Removal of the contribution of Y122• (0.13 equiv) from the spectrum of the 1.4 s timepoint (Figure 9, spectrum C), when the accumulation of **X**-Y• is maximal, reveals the broad $g = 2$ EPR spectrum of the **X**-Y• species (Figure 10A, thick solid line). As noted, this spectrum is much broader than those of Y122• (Figure 10C) and **X** (Figure 10D). Hyperfine broadening of the spectrum of an equivalent sample prepared with ^{57}Fe ($I = {}^1/_2$) demonstrates that the broad spectrum is associated with an iron species (Figure 10B). To rationalize the broad spectrum on the basis of coupling between **X** and Y122•, we have used the following spin Hamiltonian:

$$H = \beta \mathbf{H}\cdot(\mathbf{g}_1\cdot\mathbf{S}_1 + \mathbf{g}_2\cdot\mathbf{S}_2) + \mathbf{S}_1\cdot\mathbf{J}\cdot\mathbf{S}_2 + \sum_i \mathbf{S}_1\cdot\mathbf{A}_i\cdot(\mathbf{I}_H)_i \quad (1)$$

The first term represents the electronic Zeeman interactions, where $\mathbf{g}_1$ and $\mathbf{g}_2$ are the measured **g** tensors, $\mathbf{S}_1$ and $\mathbf{S}_2$ are the spins of Y122• and **X**, respectively ($S_1 = S_2 = {}^1/_2$), and **H** is the applied magnetic field. The second term represents the spin−spin interaction between the two paramagnetic centers, where

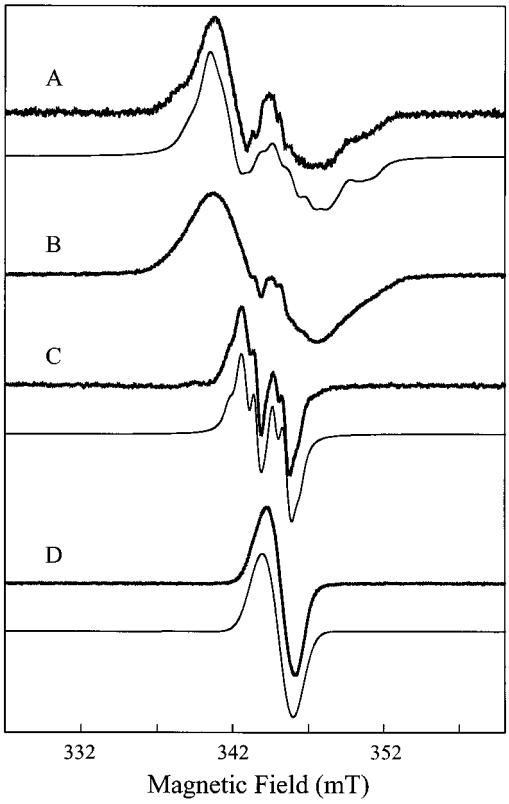

Figure 10. EPR spectra of the **X**-Y• diradical species (A and B) formed in the reaction of apo R2-W48F with Fe(II) and O_2, in comparison with (C) the EPR spectrum of Y122• formed at the completion of the reaction, and with (D) the spectrum of **X** formed in the reaction of apo R2-Y122F with Fe(II) and O_2.[14] The samples in parts A and B were prepared under identical conditions except that ^{57}Fe(II) was used in the preparation of sample B. To obtain a near-optimal accumulation of the **X**-Y• species, the reaction was quenched at 1.4 s. The contribution from the magnetically isolated Y122• (0.13 equiv) has been removed from the spectra shown in parts A and B. The instrumental settings for the EPR measurements are the same as those of Figure 9. The thin lines plotted below the experimental spectra (thick lines) are theoretical simulations using the parameters listed in Tables 1 and 2 (see text for details of the simulations).

J is the coupling tensor that includes both an isotropic exchange interaction, J_{ex}, and an anisotropic dipolar coupling $\mathbf{J}_{dipolar}$:

$$\mathbf{J} = J_{ex}\mathbf{1} + \mathbf{J}_{dipolar} \quad (2)$$

The third term of eq 1 describes the proton hyperfine interactions of the tyrosyl radical, where $(\mathbf{I}_H)_i$ represents the nuclear spin ($^1/_2$) of the *i*-th proton. X-ray crystallographic investigations of R2[3,35] indicate that the diiron cluster and Y122 are separated by a distance of about 8 Å. If these two centers retain a similar distance in R2-W48F (a reasonable assumption), the exchange interaction is expected to be small. The Mössbauer data (described below) confirm that the exchange coupling is indeed rather weak (on the order of 0.1 cm^{-1}). The effect of the isotropic exchange interaction is to split the singlet ($S = 0$) and triplet ($S = 1$) states of the coupled system. Since the probability of the transition between the singlet and triplet states is much less than those of the transitions within the triplet state, J_{ex} does not have a significant effect on the EPR spectrum. On the basis of these considerations and in an effort to minimize the number of variable parameters, we first applied the results of the

(35) Logan, D. T.; Su, X.-D.; Åberg, A.; Regnström, K.; Hajdu, J.; Eklund, H.; Nordlund, P. *Structure* **1996**, *4*, 1053−1064.

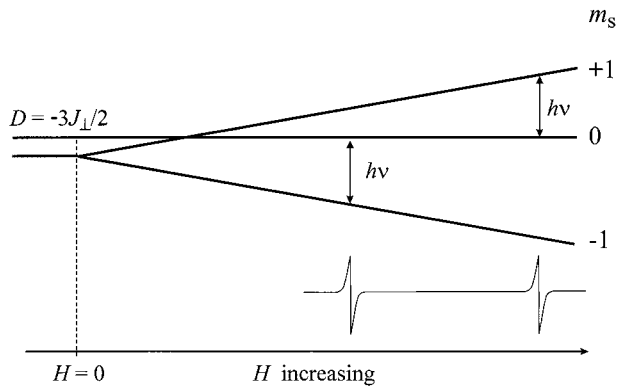

Figure 11. Energy level diagram for a triplet ($S = 1$) state with an axial zero-field splitting, and with a magnetic field (H) applied along the z-direction. The vertical arrows indicate that the allowed transitions for a constant frequency ($h\nu$) occur at two different magnetic fields, resulting in broadening of the EPR spectrum (thin solid curve).

Mössbauer analysis (see below) and fixed J_{ex} at 0.1 cm^{-1} in our analysis of the EPR spectrum. After obtaining the values for $\mathbf{J}_{dipolar}$ that best reproduce the EPR spectrum, we then performed simulations with $J_{ex} = 0.01$ cm^{-1} to confirm that the effects of J_{ex} are indeed insignificant.

The effect of the anisotropic dipolar interaction $\mathbf{J}_{dipolar}$ is to split the $S = 1$ triplet state of the coupled system. To illustrate this effect, we consider a simplified situation in which the two interacting centers are approximated by point dipoles. In such a case, the dipolar interaction is axially symmetric ($J_{xx} = J_{yy} = J_\perp$, and $J_{zz} = J_{||} - 2\,J_\perp$), and the zero-field splitting of the triplet state is given by $D = -3J_\perp/2$. An energy level diagram of a zero-field-split triplet state as a function of magnetic field applied along the z direction (Figure 11; similar effects are observed with a field applied in other directions) illustrates that the effect of zero-field splitting is to make the resonance fields for the $m_s = -1$ to $m_s = 0$ and the $m_s = 0$ to $m_s = 1$ transitions different, which, in turn, broadens the EPR spectrum. (In the absence of zero-field splitting, the two transitions would occur at the same field.) As can be seen in Figure 11, this difference in resonance fields is directly proportional to D. Consequently, the broadening of the EPR spectrum provides a very accurate measure of the strength of the dipolar coupling. Since the Zeeman effect of the triplet state depends strongly on the direction of the applied field and since the frozen sample contains randomly oriented molecules, detailed powder simulations of the EPR spectrum according to eq 1 are required to obtain quantitative information about the spin−spin interaction. At first glance, this Hamiltonian appears to contain too many parameters for a meaningful analysis. Fortunately, the magnetic parameters for intermediate **X** have been defined spectroscopically.[12−16,26,34,36] In addition, the parameters of Y122• in R2-wt have been determined by high-frequency EPR[17] and ENDOR[18] spectroscopy, and the EPR spectrum of the tyrosyl radical in R2-W48F (Figure 10C) is very similar to (though not precisely identical with) that in R2-wt. We were able, therefore, to reduce the number of variable parameters significantly by fixing the principal g values of the two paramagnetic centers and the proton hyperfine coupling tensors of the tyrosyl radical at (or very near) the previously determined values (Table 1). The EPR spectra of magnetically isolated Y122• and **X** simulated with these parameters (Figure 10, thin lines in C and D, respectively) agree well with the corresponding experimental spectra. Because the **g** tensors for the two interacting centers are nearly isotropic, the angular orientation of the principal axes of the two tensors has an insignificant effect on the EPR spectrum of the interacting system. This permits a further reduction in the number of variable parameters by assumption of collinear orientation of the **g** tensors. Consequently, the only variable parameters in our analysis are the three principal components of $\mathbf{J}_{dipolar}$. The EPR spectrum simulated (Figure 10A, thin line) with the values obtained for $\mathbf{J}_{dipolar}$ (Table 2) agrees very well with the experimentally determined spectrum of the **X**-Y• species.

Table 1. Electronic g Values for **X** and Y122• and Proton Hyperfine Coupling Constants for Y122• in R2-W48F

	X[a]	Y122•[b]	
g_x[c]	2.007	2.00912	
g_y[c]	1.999	2.00457	
g_z[c]	1.994	2.00225	
proton[c]	H-3 (5)		H-β
A_{xx} (MHz)	26.9		57.8
A_{yy} (MHz)	7.8		52.1
A_{zz} (MHz)	19.6		54.9

[a] Reference 16. [b] The values are slightly modified from those of refs 17 and 18 to fit the EPR spectrum of Y122• in R2-W48F. [c] The principal axis systems for the **g** tensors are assumed to be collinear. The z-axis is perpendicular to the plane of the phenyl ring and the x-axis along the C-4 to oxygen bond of Y122 as defined in ref 18. The hyperfine couplings for protons H-2 and H-6 are very weak and have been neglected in our analysis. One of the two β protons is weakly coupled to the electronic spin and has also been neglected in this analysis. As in ref 18, the principal axis systems for H-3 and H-5 are rotated, respectively, by 30° and 150° along the z-axis of the **g** tensor.

Table 2. Comparison of Experimentally Determined $\mathbf{J}_{dipolar}$ for the Spin−Spin Coupled **X**-Y• with Values Calculated by Using the Point Dipole Approximation

	exptl	theory[a]		
r (Å)		7	8	9
J_{xx} (cm^{-1})	0.0025	0.0050	0.0034	0.0024
J_{yy} (cm^{-1})	0.0045	0.0050	0.0034	0.0024
J_{zz} (cm^{-1})	−0.0070	−0.0100	−0.0068	−0.0048

[a] An angle of 71° between the displacement vector **r** and the normal of the Y122 plane (the z-axis) is used in these calculations. This value is obtained based on the X-ray crystallographic data of met R2.[3]

To examine whether the obtained $\mathbf{J}_{dipolar}$ is consistent with the expected distance between the two interacting spins, we applied a point dipole model (eq 3) to estimate the dipolar coupling strength as a function of the distance vector **r** connecting the two interacting spins S_1 and S_2, where β is the Bohr magneton. The results of the estimates for $r = 7$, 8, and

$$\mathbf{J}_{dipolar} = \frac{\beta^2}{r^3}\left[\mathbf{g}_1\cdot\mathbf{g}_2 - \frac{3(\mathbf{g}_1\cdot\mathbf{r})(\mathbf{r}\cdot\mathbf{g}_2)}{r^2}\right] \qquad (3)$$

9 Å are compared in Table 2 with the experimentally determined $\mathbf{J}_{dipolar}$. The experimental values compare very well with the estimated strength for $r = 8$ Å. X-ray crystallographic data for met R2[3] indicate a distance of 7.7 Å between the C4 of Y122 and the midpoint of the Fe− Fe vector. Therefore, the values obtained for $\mathbf{J}_{dipolar}$ are consistent with the expected distance between the two interacting spins. As mentioned above, a point dipole−point dipole interaction results in axially symmetric **J** tensors (Table 2). The observed EPR spectrum of **X**-Y• cannot, however, be simulated with an axial **J**, indicating (as expected) that the spins of the two interacting centers are delocalized.

The effects of the spin−spin interaction are also quite clearly seen in the Mössbauer spectra of **X** in the **X**-Y• species. A sample freeze-quenched at 1.7 s yielded the spectra shown in

(36) Bollinger, J. M., Jr.; Stubbe, J.; Huynh, B. H.; Edmondson, D. E. *J. Am. Chem. Soc.* **1991**, *113*, 6289−6291.

Figure 7, which were recorded at 4.2 K with an applied field of 50 mT (A) or 8 T (B). The solid lines in Figure 7 are the theoretical simulations of **X** obtained with the spin Hamiltonian shown in eq 4 and $J = 0$ (i.e. magnetically isolated **X**). The

$$H = \beta \mathbf{H}\cdot(\mathbf{g}_1\cdot\mathbf{S}_1 + \mathbf{g}_2\cdot\mathbf{S}_2) + \mathbf{S}_1\cdot\mathbf{J}\cdot\mathbf{S}_2 + \sum_{i=1}^{2}\mathbf{S}_1\cdot\mathbf{A}_i\cdot\mathbf{I}_i + H_Q \quad (4)$$

first two terms in eq 4 have the same meaning as in eq 1. The third term describes the magnetic hyperfine interactions between the diiron cluster spin S_1 and the nuclear spins I_1 and I_2 of the two iron nuclei. The fourth term is the quadrupole interactions at the two iron nuclei, which can be written as eq 5 where $(V_{xx})_i$, $(V_{yy})_i$, and $(V_{zz})_i$ are the principal components of the electric field gradient tensor of the i-th iron site and the asymmetry parameter, η_i, is equal to $[(V_{xx})_i - (V_{yy})_i]/(V_{zz})_i$. As noted, the

$$H_Q = \sum_{i=1}^{2}\frac{eQ(V_{zz})_i}{12}[3\mathbf{I}_{zi}^2 + I_i(I_i+1) + \eta_i(\mathbf{I}_{xi}^2 - \mathbf{I}_{yi}^2)] \quad (5)$$

characteristic features of the paramagnetic **X** are clearly identifiable in the experimental spectra, indicating unambiguously the presence of **X** at a reaction time of 1.7 s. However, to match the absorption intensity of these features, the theoretical simulation for the 50-mT spectrum (Figure 7A) can account for only 20% of the total iron absorption, whereas the simulation for the 8-T spectrum (Figure 7B) can account for 38% of the total iron absorption. For magnetically isolated **X**, the internal fields at the iron sites will reach their saturation values with the application of even a weak field (such as 50 mT), because **X** has a spin of $^1/_2$ and a doubly degenerate electronic state. Consequently, if **X** is magnetically isolated, the above analysis should yield identical quantitation for **X** in spectra recorded at different field strengths. The observed discrepancy indicates that about half of the population of **X** in the 1.7-s sample does not exhibit magnetically split spectra under the application of a weak field. This observation is consistent with the interaction of **X** with a nearby paramagnetic center, presumably Y122$^\bullet$, as suggested by the EPR data.

An energy level diagram of an $S=^1/_2 - S=^1/_2$ coupled system as a function of the strength of a magnetic field applied in the z-direction (Figure 12A; as before, similar results are obtained with fields applied in other directions) illustrates this point. In this plot, a $J_{ex} = 0.1$ cm^{-1} and the $\mathbf{J}_{dipolar}$ obtained from the EPR analysis (see above) have been used. The coupled system consists of four states (a singlet $S = 0$ state and a zero-field-split triplet $S = 1$ state), which are labeled as φ_1, φ_2, φ_3, and φ_4. With a weak applied field, such as 50 mT, the spin expectation values at the diiron cluster are practically zero for states φ_2 and φ_3 (Figure 12B). Since the internal field is directly proportional to the spin expectation value, these two states will not generate internal fields at the two iron nuclei of **X** under the application of a weak magnetic field. On the other hand, the spin expectation values for states φ_1 and φ_4 are saturated ($-^1/_2$ and $+^1/_2$, respectively) with a weak applied magnetic field. In other words, fully saturated internal fields are generated at the iron nuclei of **X** for states φ_1 and φ_4. Consequently, if all four states are populated under the application of a weak magnetic field, the corresponding Mössbauer spectrum will consist of both magnetically split spectral components from states φ_1 and φ_4 and quadrupole-doublet components from states φ_2 and φ_3. As mentioned above, at 4.2 K and with a 50 mT applied field, only about half of the population of **X** exhibits the magnetically split spectrum. Thus, the other half of the

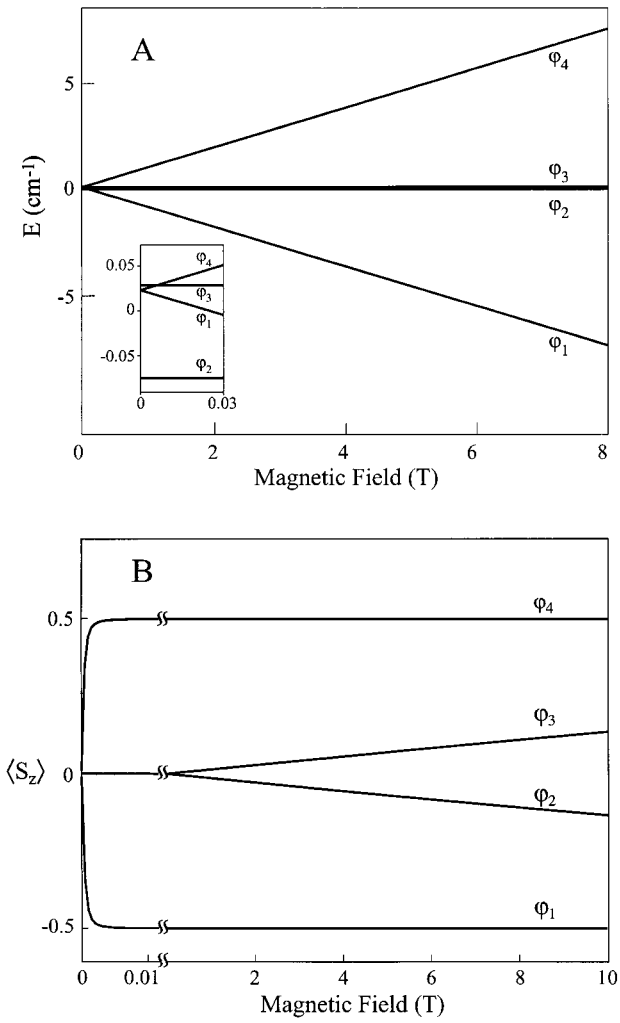

Figure 12. Energy level diagram (A) and spin expectation values (B) of an $S=^1/_2 - S=^1/_2$ coupled system as functions of a magnetic field applied along the z-direction. The parameters listed in Table 2 for $\mathbf{J}_{dipolar}$ and $J_{ex} = 0.1$ cm^{-1} are used for this graph.

population must exhibit a quadrupole doublet spectrum. In other words, under these conditions all four states are almost equally populated. Consequently, the J_{ex} must be much smaller than kT at 4.2 K (2.92 cm^{-1}). With strong magnetic fields (such as 8 T), the states are split by the Zeeman interaction (see Figure 12A) and only the state φ_1 is significantly populated at 4.2 K. Consequently, fully saturated internal fields are generated at both iron sites creating a situation resembling that of a magnetically isolated **X**.

To demonstrate quantitatively the validity of the above argument and to characterize the **X**-Y$^\bullet$ further, we have used eq 4 to analyze the Mössbauer spectra of **X**-Y$^\bullet$ in the 1.7-s sample recorded at various applied fields. Figure 13 shows the spectra of **X**-Y$^\bullet$ recorded at 4.2 K with a magnetic field of 50 mT (A), 3 T (B), or 8 T (C) applied parallel to the γ-beam. These spectra were prepared by removing the contributions of species other than **X**-Y$^\bullet$ from the raw data (see the legend of Figure 13 for details). The 50 mT spectrum of **X** is a superposition of a magnetically split component and a central component consisting of quadrupole doublets. The intensities of the two components are nearly equal. At 3 T, the intensity of the central component is reduced, and at 8 T only a magnetically split component is observed. This observation is consistent with the involvement of **X** in a weak spin−spin interaction, as delineated in the preceding paragraphs. Theoreti-

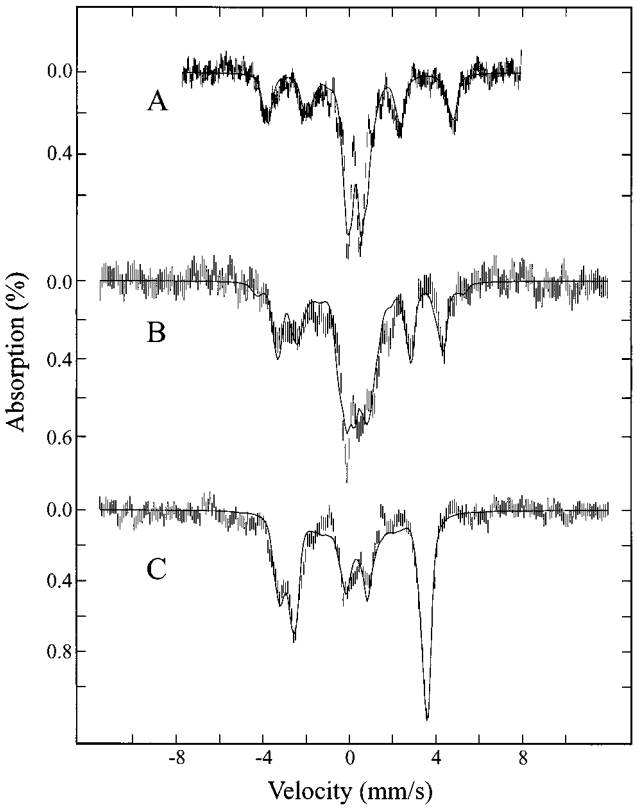

Figure 13. Mössbauer spectra of the **X**-Y• species at 4.2 K with a magnetic field of 50 mT (A), 3 T (B), and 8 T(C) applied parallel to the γ-beam. Analysis of the Mössbauer data indicates that multiple products are generated in the reaction of R2-W48F with Fe(II) and O_2.[32] In addition to the μ-oxo-diiron(III) cluster, two other diferric clusters with distinct Mössbauer parameters (diferric 1: $\Delta E_Q = 0.64$ mm/s and $\delta = 0.52$ mm/s; diferric 2: $\Delta E_Q = 1.46$ mm/s and $\delta = 0.5$ mm/s) are produced. Mononuclear ferric species are also detected. The 1.7-s sample was found to contain 13% unreacted diferrous clusters, 12% wild-type μ-oxo-diiron(III) clusters, 14% diferric 1, 4% diferric 2, and 19% mononuclear ferric species. Contributions from these species were removed from the raw data to reveal the spectra of **X**-Y• shown in this figure. The solid lines are theoretical simulations using parameters listed in Tables 1 and 2 and $J_{ex} = 0.1$ cm^{-1}.

cal simulations (solid lines plotted over the data) according to eq 4 and the parameters listed in Table 3 faithfully reproduce the experimental spectra. (Note that the parameters that best reproduce the spectra of **X** in R2-W48F are slightly different from those associated with **X** in R2-wt[16]). The analysis shows that the spin−spin interaction between **X** and Y122• is indeed weak, with an isotropic J_{ex} of 0.1−1 cm^{-1}. Within this range of J_{ex}, the small anisotropic $\mathbf{J}_{dipolar}$ determined from the EPR analysis has an insignificant effect on the simulated Mössbauer spectra. Best agreement between the experimental spectra and the theoretical simulations was obtained with $J_{ex} = 0.1$ cm^{-1}. The theoretical spectra plotted in Figure 13 are simulated with $\mathbf{J}_{dipolar}$ obtained from the EPR analysis and $J_{ex} = 0.1$ cm^{-1}.

The presence of a small exchange interaction on the order of 0.1 cm^{-1} may suggest a through-bond pathway between Y122• and **X**. In proteins, exchange interactions of this magnitude are not unusual for paramagnetic centers interacting at distances comparable to that expected between the constituents of the **X**-Y• species.[37−41] For example, the S_2Yz• EPR signal in photosystem II has been explained as the result of a spin−spin interaction between the Mn_4 cluster and Yz• with a dipolar interaction corresponding to an inter-center distance of 7.7 Å and an exchange interaction of about 0.06 cm^{-1}.[37−40] Due to the presence of the altered iron products in our freeze-quenched Mössbauer samples, the determination of J_{ex} for the **X**-Y• intermediate contains a large uncertainty. The value of 0.1 cm^{-1} for J_{ex} used in the analysis is an order-of-magnitude estimate. However, it warrants emphasis that cases with and without a spin−spin interaction are readily distinguishable physical situations (as described in the preceding paragraphs) and that the Mössbauer data unambiguously establish both that **X** is magnetically coupled to another paramagnetic center and that the coupling is weak. Considering that the optical data show the presence of Y122• and that the EPR data can be reproduced by assuming a spin−spin coupled **X** and Y122•, the most reasonable candidate for the paramagnetic center that couples with **X** is the tyrosyl radical.

Table 3. Comparison of Mössbauer Parameters for the Diiron Intermediate **X** in Wild-type R2 and in R2-W48F[a]

	R2[b]		W48F-R2	
Fe site	1	2	1	2
δ (mm/s)	0.56 (3)	0.26 (4)	0.47 (5)	0.22 (5)
ΔE_Q (mm/s)	−0.9 (1)	−0.64	−0.7 (1)	−0.64 (10)
η	0.5	2.7	0.5	2.7
$A_{xx}/g_n\beta_n$ (T)	−53.0 (5)	27.0 (2)	−53.0 (5)	29.0 (10)
$A_{yy}/g_n\beta_n$ (T)	−53.0 (5)	27.0 (2)	−53.0 (5)	24.0 (10)
$A_{zz}/g_n\beta_n$ (T)	−53.0 (5)	20.0 (2)	−52.0 (10)	24.0 (10)

[a] Values in parentheses represent uncertainties of the last significant digit(s). [b] Reference 16.

In summary, the kinetic data obtained by three different spectroscopic methods, stopped-flow absorption and freeze-quench EPR and Mössbauer spectroscopies, show simultaneous formation of **X** and Y122•. Unique EPR and Mössbauer spectroscopic features indicate that the concomitantly forming **X** and Y122• interact magnetically at a submolecular distance. This requires that **X** and Y122• be present *simultaneously in the same molecule*. In other words, the spectroscopic data establish firmly that in the reaction of R2-W48F with Fe(II) and O_2, **X** and Y122• form concomitantly.

Nature of the Precursor to the X-Y• Diradical Species. As noted, the timecourses of Y122• formation at different O_2 concentrations suggest that a prior intermediate accumulates. One possible identity of this species is a noncovalent complex between the Fe(II)-R2-W48F and O_2 that forms prior to rate-limiting O_2 activation. A chemical quench experiment was performed to evaluate this possibility. Fe(II)-R2-W48F was mixed at 5 °C with an equivalent volume of O_2-saturated buffer, and the reaction was quenched with acid after variable reaction time. The fraction of Fe(II) that had been oxidized in a given time point was determined by comparison of the quantity of Fe(II)-ferrozine$_3$ complex (as reported by A_{562}) that could be formed after the quench to the quantity formed after reduction of all Fe(III) back to Fe(II) with ascorbate. The kinetics of Fe(II) oxidation are apparently multiphasic (Figure 14), with the best-fit rate constant for the fastest phase (38 ± 6 s^{-1}) agreeing well with k_{obs} for the lag phase of Y122• formation observed by stopped-flow (38 ± 3 s^{-1} at this [O_2]). The amplitude of this phase corresponds to oxidation of 1.72 ± 0.13 equiv of

(37) Lakshmi, K. V.; Eaton, S. S.; Eaton, G. R.; Frank, H. A.; Brudvig, G. W. *J. Phys. Chem. B* **1998**, *102*, 8327−8335.
(38) Astashkin, A. V.; Mino, H.; Kawamori, A.; Ono, T.-A. *Chem. Phys. Lett.* **1997**, *272*, 506−516.
(39) MacLachlan, D. J.; Nugent, J. H. A.; Warden, J. T.; Evans, M. C. W. *Biochim. Biophys. Acta* **1994**, *1188*, 325−334.
(40) Peloquin, J. M.; Campbell, K. A.; Britt, D. A. *J. Am. Chem. Soc.* **1998**, *120*, 6840−6841.
(41) Sanakis, Y.; Petasis, D.; Petrouleas, V.; Hendrich, M. *J. Am. Chem. Soc.* **1999**, *121*, 1.

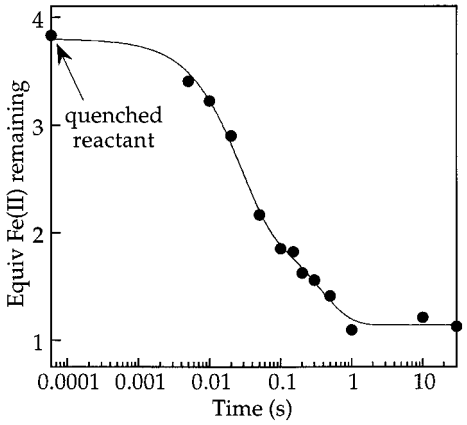

Figure 14. Kinetics of Fe(II) oxidation after 1:1 mixing of the Fe(II)-R2-W48F complex (4.0 equiv, 0.5 mM intitial protein concentration) with O_2-saturated (at 25 °C) buffer B. The experimental procedure is described in detail in the Materials and Methods section. The solid line is a fit of the equation for two parallel first-order decay processes to the data. It corresponds to $k_1 = 38\ s^{-1}$, amplitude$_1$ = 1.7 equiv, $k_2 = 2.8\ s^{-1}$, amplitude$_2$ = 0.93 equiv, and 1.14 equiv of Fe(II) at completion. The latter value implies that 2.86 equiv of Fe(II) are oxidized, which agrees well with the values from the aerobic Fe(II) titrations.

Fe(II) (or 0.86 ± 0.07 equiv of diiron(II) cluster). This quantity is sufficient to account for the primary reaction pathway in which a maximum of 0.6−0.76 equiv of Y122$^\bullet$ accumulates. Thus, the results provide additional evidence for the inferred intermediate and suggest that it is probably a covalent complex with O_2 in which the Fe(II) of the reactant has undergone oxidation. Caution is appropriate in interpretation of these results, however, because of the possibility that high-valent Fe or partially reduced oxygen species present at the time of the acid quench might react further (possibly by oxidation of additional Fe(II)) after quenching. In addition, the origin of the second phase is not obvious.

The combined chemical, kinetic, and spectroscopic characterization of the R2-W48F reaction suggest a mechanism involving accumulation of an $(Fe_2O_2)^{4+}$ species, which is more reactive toward one-electron reduction than cluster **X**, as a direct consequence of the absence of the electron-shuttling residue W48. This intermediate directly oxidizes Y122, producing the **X**-Y$^\bullet$ species. This step leaves both oxidizing equivalents of the $(Fe_2O_2)^{4+}$ species still in close proximity. Unable to facilitate reduction of **X**, the protein instead permits further reaction between the adjacent oxidized constituents and, consequently, is very inefficient at generating stable Y122$^\bullet$ unless it is aided in reductive quenching of **X** by a strong reductant.

Acknowledgment. This work was supported by NIH grants GM55365 (J.M.B.) and GM47295 (B.H.H. and D.E.E.) and by grants from the Searle Scholars Program of the Chicago Community Trust and the Camille and Henry Dreyfus Foundation (to J.M.B.).

Supporting Information Available: Detailed procedures used to verify that Fe is incorporated into R2-W48F produced after addition of phenanthroline but not into R2-W48F produced in the absence of phenanthroline and a procedure to demonstrate that R2-W48F undergoes oxidative inactivation (PDF). This material is available free of charge via the Internet at http://pubs.acs.org.

JA001279M